COBEM 2023 27TH INTERNATIONAL CONGRESS OF MECHANICAL ENGENEERING

ABCM Brazilian Society of Mechanical Sciences and Engineering
27th ABCM International Congress of Mechanical Engineering
December 04-08, 2023, Florianópolis-SC, Brazil

COB-2023-0940
CFD SIMULATIONS FOR OBTAINING STEADY-STATE HYDRODYNAMIC PARAMETERS OF A FIVE-DEGREE-OF-FREEDOM ROV WITH JET PROPULSION

Arthur Sena Marques
Hélio Valdevieso Catarin
Federal University of Santa Catarina - Estr. Dona Francisca, 8300 - Bloco U - Zona Industrial Norte, Joinville - SC, 89219-600
ar.se.marques@gmail.com, heliovcatarin@gmail.com.

Lucas Weihmann
Federal University of Santa Catarina - Estr. Dona Francisca, 8300 - Bloco U - Zona Industrial Norte, Joinville - SC, 89219-600
lucas.weihmann@ufsc.br.

Andrea Piga Carboni
Federal University of Santa Catarina - Estr. Dona Francisca, 8300 - Bloco U - Zona Industrial Norte, Joinville - SC, 89219-600
andrea.piga@ufsc.br.

Abstract. *The difficulty of accessing tools and resources required for underwater work remains a challenging task for humans due to physical limitations and safety issues. In this context, unmanned underwater vehicles such as remotely operated vehicles (ROVs) have become essential tools for various purposes. Depending on the service mission, ROVs can be designed for exploration of resources at great ocean depths, maintenance and repair of ship hulls, and marine monitoring and research activities. Obtaining the resistance to advance of complex geometry underwater vehicles through analytical methods can be a difficult and often impossible task. Therefore, a better understanding of drag force can be achieved through the use of computational fluid dynamics (CFD) simulations. In this study, a five-degree-of-freedom ROV designed to act as an underwater platform with jet propulsion was examined, which can be used as a submersible base for manipulator support in the future. The objective of this work was to obtain the steady-state hydrodynamic parameters of the main translation movements of the ROV, including the intermediate direction between the roll and pitch axes of the vehicle. To achieve this objective, drag force was calculated as a function of the ROV velocity and angle of incidence, and the results were presented through two-dimensional and three-dimensional graphs. The study also addressed additional mesh controls due to the geometric complexity of the model, a quality assessment of the mesh generated and used in the final analyses of this work, as well as the evaluated parameters that had the greatest influence on the final results. The conclusions of this study discuss possible future work related to obtaining precise hydrodynamic parameters and an accurate control system for generic transient states. The results of this study demonstrate the effectiveness of using CFD simulations to better understand the hydrodynamic behavior of complex underwater vehicles, which can contribute to the development of more efficient and high-performance designs.*

Keywords: *ROV, CFD, Drag force.*

1. INTRODUCTION

The utilization of unmanned underwater vehicles, such as remotely operated vehicles (ROVs) and autonomous underwater vehicles (AUVs), has emerged as a significant tool for companies and professionals engaged in fields including deep-sea resource exploration, ship hull maintenance and repair, and marine monitoring and research activities (Yuh, 2000). These vehicles are employed in tasks that entail potential hazards to human life, necessitate cost reduction, or are constrained by physical or human limitations (Tavares, 2005; Zanoni, 2012).

It is within this scenario that the project of a five-degree-of-freedom ROV is being developed by a group of students and researchers at the CTJ (Technological Center of Joinville) of UFSC (Federal University of Santa Catarina). The work, conducted by authors Marques and Catarin (2020), was initiated with the preliminary objective of designing and constructing an underwater vehicle with waterjet propulsion, aiming to serve as a platform for future robotic arm support. The vehicle model is depicted in Figure 1.

In order to obtain a representative hydrodynamic model of the system, which can be subsequently used in the control system, this work focuses on identifying and obtaining the steady-state hydrodynamic parameters of this ROV through the use of simulations and Computational Fluid Dynamics (CFD) analyses, as defined by Hu (2008) and similarly to what was done previously by Ramírez-Macias et al. (2016) and Celly et al. (2019), employing the finite volume method (Muniz, 1995; Fox, 2011).

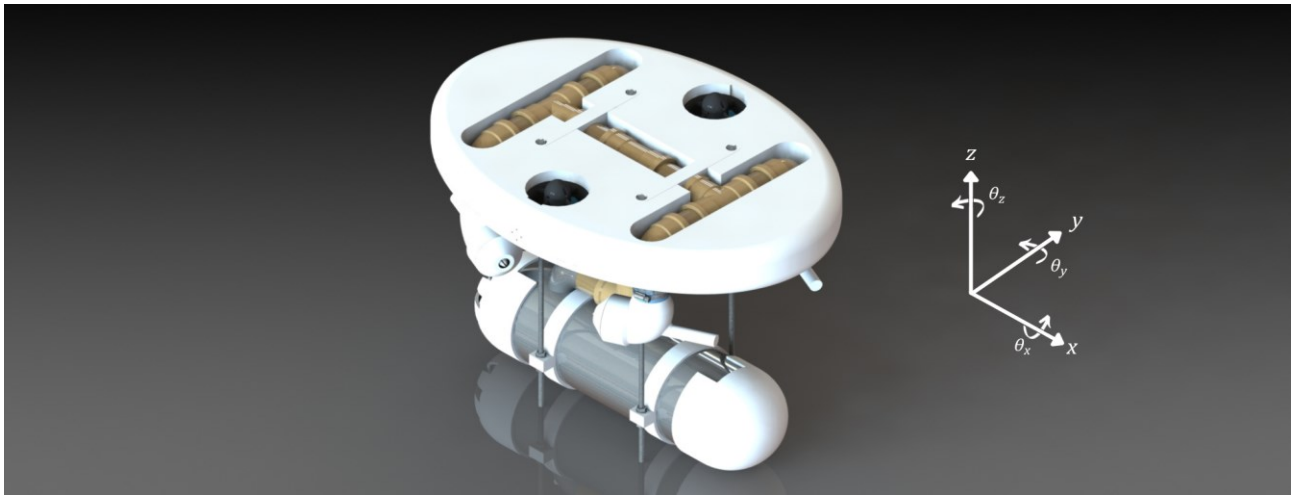

Figure 1. Model of the prototype of the ROV developed at CTJ of UFSC. Source: Marques and Catarin (2020, p. 51).

1.1 Coordinate system

According to Grewal et al. (2001), the coordinate systems used in inertial navigation primarily consist of spherical coordinate systems. The RPY (Roll-Pitch-Yaw) coordinate system is employed as the platform's navigation system, with axes fixed to the vehicle. The x-axis (roll axis) is oriented in the nominal direction of the vehicle, the longitudinal axis (the platform's longest dimension). The z-axis (yaw axis) is oriented perpendicular to the platform's surface, pointing upward, and the y-axis (pitch axis) is determined following the right-hand rule. The RPY coordinate system, in turn, is referenced to a local ENU (East-North-Up) navigation system. Surge, sway, and heave are the degrees of freedom related to translation along the orthogonal coordinate axes *x*, *y*, and *z*, and roll, pitch, and yaw are the degrees of freedom related to rotation, θ_x, θ_y *e* θ_z, around the *x*, *y*, and *z* axes, respectively, as illustrated in Figure 1.

1.2 Platform propulsion system

The propulsion system of the platform, for the initial 5 DOF, is essentially composed of four subsystems: Pump, Piping, Propellers, and Jet propulsion system. The jets are designed to receive the water flow from the piping system and expel it through the nozzle to provide thrust to the ROV.

Out of the five degrees of freedom studied so far in the project, three of them are attributed to the force generated by the jets, namely, surge, sway, and yaw. Thus, by following the configuration of four nozzles, enumerated as shown in Figure 2.a, it is possible to achieve surge motion by activating (either fully or partially) nozzles 2 and 4, for instance. In this case, if the nozzles are opened in equal proportions, the forces generated in the y-direction by the two nozzles will cancel out, resulting in motion only in the x-direction. Similarly, sway motion can be obtained by opening nozzles 1 and 2 or 3 and 4 equally. Any non-equal configuration of nozzle opening would generate motion in both the *x* and *y* directions. Following this logic, rotation around the z-axis of the platform (yaw) can be generated through the torque generated between nozzles 1 and 4, for example (Figure 2.b).

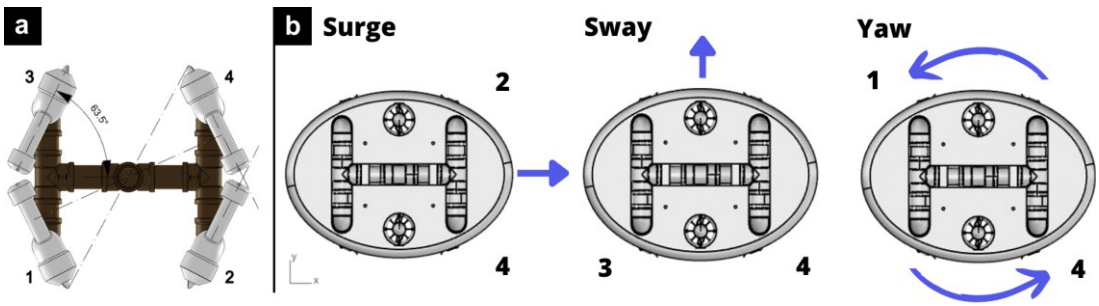

Figure 2. Fictional numbering of nozzles (bottom view) (a) and examples of nozzle opening configurations and their resulting movements (top view) (b). Source: Adapted from Marques (2022, p. 21 and 22).

For the calculations performed by Marques and Catarin (2022) based on the configurations, simplifications, and data from the previously mentioned pump, the maximum velocity obtained for both the surge and sway movements is approximately 0.9 m/s.

2. SIMULATION

STAR-CCM+ is a Computer-Aided Engineering (CAE) tool developed to solve multidisciplinary problems in fluid and solid mechanics within a single integrated interface. It is primarily used to solve problems involving flow and heat transfer (Siemens, 2021). Due to its integrated and user-friendly interface, it provides easy understanding and learning, making it the software to be used for the simulations in the subsequent stages of this work. Its utilization was made possible through the availability of licenses in the Naval Simulation Laboratory (LaSiN) and the Subaquatic Technology Laboratory (LaSub), at CTJ-UFSC.

The objective of the simulations, as previously mentioned, is to obtain drag forces for different platform motion configurations. In addition to motions in the orthogonal directions, x, y, and z, the aim is also to determine the drag, in steady-state, along an intermediate direction between x and y identified by the angle ϕ, similarly to employed by Ramírez-Macias et al. (2019), as shown in Figure 3.

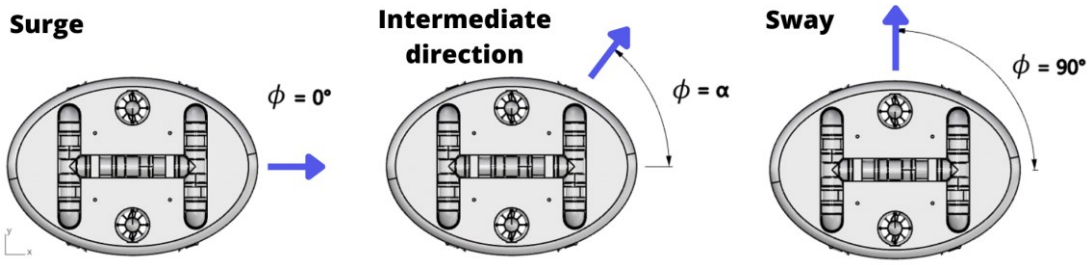

Figure 3. Types of platform motion. Source: Adapted from Marques (2022, p. 34).

Next, the aim is to vary the platform velocity between two limiting values, with a defined and constant increment, in order to obtain the drag force for each velocity, for a consistent initial configuration of motion. This process allows for the establishment of a polynomial curve that represents the drag force as a function of velocity, for a given angle ϕ, based on the obtained data points (F_d, V), where F_d represents the drag force and V represents the relative velocity between the fluid and the analyzed body.

Since the drag force also depends on the analyzed angle, a more comprehensive representation of this force is obtained by considering a surface as a function of V and ϕ. Therefore, given that the platform is moving at a constant angle ϕ and a relative velocity V, the drag force of the platform can be determined for any point on this surface as a function f, where f represents the equation governing this surface.

Due to the lack of comparison data for this specific ROV format in the literature, the validation stage, essential in any simulation work, compared experimental results of drag coefficients for flow around spheres in different Reynolds ranges with the author's simulation results. For the laminar regime (Reynolds 100 and 300), data from Constantinescu and Squires (2000) and Kim and Choi (2002), among others, were used, with relative errors ranging from 0.46% to 3.99%. For the turbulent regime (Reynolds $1.1x10^6$), data from Achenbach (1972) and Constantinescu et al. (2002) were used, with relative errors ranging from 10% to 28.57%.

2.1 Pre-processing

2.1.1 Domain definition

The physical space to be simulated, according to the design requirements, is referred to as the simulation domain. This domain can include the geometry of the real-world system, its contents, and the surrounding environment (Siemens, 2021). Thus, the domain represents the environment where the fluid used in the analysis resides and where the object under investigation is positioned. The three-dimensional size of the domain must be sufficiently large to accommodate the object and provide results that closely approximate reality. In this work, dimensions approximately 20 times the length, width, and height of the ROV are employed (Chin and Lau, 2012). The Figure 4 below illustrates the domain used in the final simulations, its dimensions, and the names assigned to each of its faces.

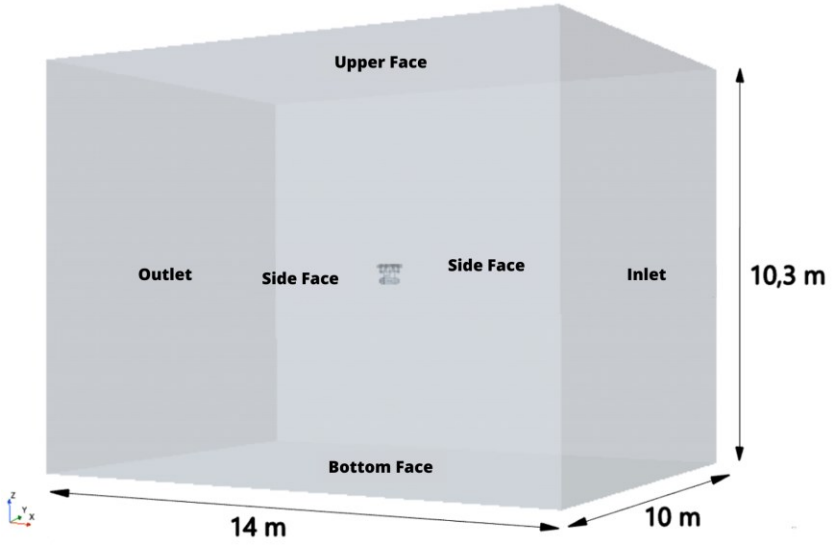

Figure 4. Domain used in the simulations and its dimensions. Source: Adapted from Marques (2022, p. 34)

2.1.2 Definition of the physical models

The configuration of the physical models defines the primary variables of the simulation and the mathematical formulations employed in the solution process (Siemens, 2021). It is important, in this context, to select the physical models that best fit and represent reality in a particular analysis. For the resolution of fluid motion equations, the RANS (Reynolds-averaged Navier-Stokes) model was employed. Table 1, below, identifies the selected physical models for the platform analysis.

Table 1 – Selected physical models

Type of selection	Physical model
Space	Three-dimensional
Material	Liquid: H_2O
Type of flux	Segregated Flux
Equation of state	Constant density
Time	Permanent regime
Viscous regime	Turbulent
Average turbulence of Reynolds	K-Epsilon Turbulence
Optional model	Interpolation of the solution – Nearest neighbor

Usually in simulations, it is easier to make the fluid move at a constant velocity in the opposite direction to the stationary ROV, rather than making the ROV move forward at a constant velocity while the fluid domain remains stationary without current flow. Since drag force depends only on the relative motion between the body and the fluid, the result obtained from both simulations is the same (Chin and Lau, 2012). A comparison between the two cases can be seen in Figure 5.

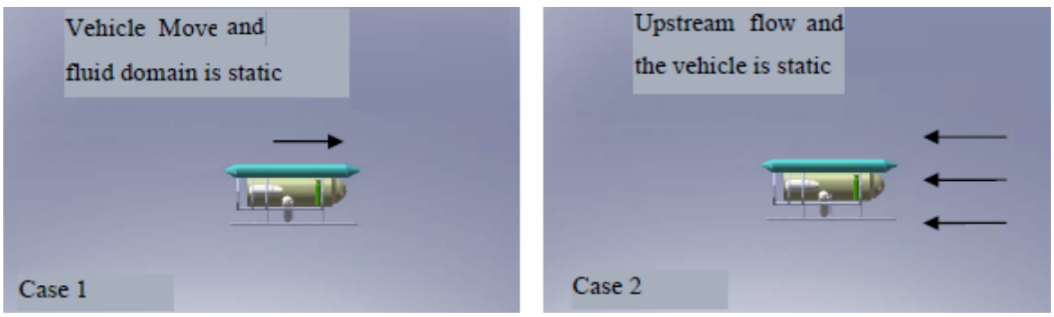

Figure 5. Comparison between fluid motion and ROV motion. Source: Chin and Lau (2012, p. 5).

The advantage of keeping the ROV static is that the boundary conditions can be set up more easily for the simulation without altering the domain, for example. On the other hand, moving the ROV would create more complex and dynamically changing meshes, making it more challenging to handle and requiring higher computational power (Chin and Lau, 2012).

2.1.3 Region settings

The inlet, top, bottom, and side faces were all defined as *Velocity Inlet*, with flow running in the x-direction parallel to the faces (Gong et al., 2022). This configuration allows each face to be treated by the software as an open domain with a constant velocity inlet in the flow direction, perpendicular only to the inlet face. The outlet face is defined as *Pressure Outlet*. Finally, the *Wall* configuration is applied to the external surface of the ROV body. This configuration applies all the necessary conditions for the software to treat the ROV as an impermeable wall, representing constraints on movement and providing the required no-slip condition for calculations (Siemens, 2021).

According to Chin and Lau (2012), most ROV operations, considering their scale and velocity, have Reynolds numbers typically greater than $1{,}1x10^6$, indicating turbulent flow. In this regard, another parameter that deserves attention is the turbulence intensity. For flows around cars, submarines, and airplanes in stationary fluid domains, low turbulence cases with intensities less than 1% are usually encountered. For ROVs, this value can be even lower, as in the case adopted by the author at 0.1% (Chin and Lau, 2012). To maintain a reasonable safety margin, considering the complexity of the ROV geometry, a turbulence intensity of 1% was chosen.

2.1.4 Mesh generation and additional controls

The solvers of STAR-CCM+ compute solutions for physical equations at locations defined by the mesh. For Finite Volume, the software calculates the values at the cell centers (Siemens, 2021). Thus, the software solvers are responsible for locally solving the equations based on the mesh elements, and the mesh itself plays a crucial role in delivering simulation results with varying levels of accuracy. Therefore, it is necessary to conduct a thorough study of the mesh quality for the analysis. The meshing tools, or mesh generators, selected for this purpose are: Trimmed cell mesher, Surface remesher, Automatic surface repair, and Prism layer mesher.

Additional controls, or customizable controls, take precedence over standard controls for surface or volume modelers. The following controls were applied in this case:

- The standard target surface size for the domain faces was set at 5000% of the base cell size. An illustration of the before and after effect of the additional *domain control* applied to a mesh can be seen in Figure 6.

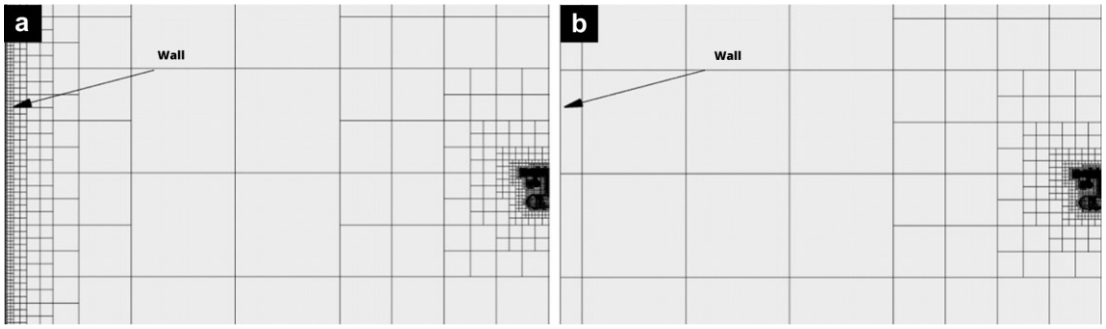

Figure 6. Before (a) and after applying the domain control (b). Adapted from Marques (2022, p. 49).

- The *wake refinement control* aims to refine the mesh in the wake formed behind the ROV body, in order to model the effects of turbulence and potential flow alterations that could affect the body's drag. This makes the simulation closer to reality. It was defined to be equivalent to three times the total length of the analyzed body, i.e., 2.1 m, with other characteristic dimensions similar to the body.

- The *volumetric control* applies mesh refinement in volumetric regions that require more precise control, either due to having more protrusions, notches, or curvatures. In total, four cylinders completely covering the nozzles, two spheres covering the propellers, and one sphere covering the rear casing of the pump, which has openings for water passage, are applied. The standard for volume control was adopted at 50% of the base size, and the arrangement of control cylinders and spheres can be seen in Figure 7.

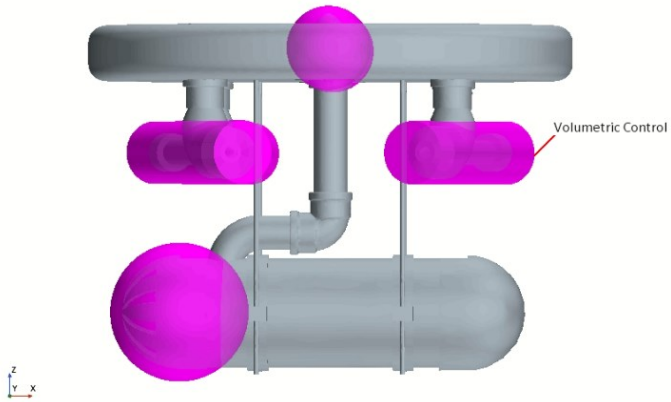

Figure 7. Arrangement of cylinders and spheres in the volume control. Source: Marques (2022, p. 51).

2.1.5 Mesh quality

In general, a low-quality volumetric mesh can reduce the accuracy and efficiency of the obtained solution (Siemens, 2021). Therefore, it is necessary to conduct a study on the mesh quality of the analysis. The study was carried out through simulations, tests, and comparisons involving the following parameters: Base cell size, Surface growth rate, Volumetric growth rate, Wake refinement, and number of prism layers.

The conducted tests involve numerical modifications in one or more of the parameters that will be discussed, while keeping the average or default settings as the baseline, typically suggested by STAR-CCM+. Additionally, the configurations for the additional controls remain as previously defined, and the inlet velocity in each cell is set to 0.9 m/s, matching the maximum velocity previously found by the authors Marques and Catarin (2020). The tests compare both the impact of a parameter on a single base cell size and the impact it has on different base cell sizes. The varied values for each parameter are shown in Table 2 below:

Table 2. Numerical variation of the analyzed parameters

Parameter	Var. 1	Var. 2	Var. 3
Base cell size	35 mm	28 mm	21 mm
Surface growth rate	1,425	1,3	1,1
Volumetric growth rate	1	2	4
Wake refinement	100%	50%	25%
Number of prism layers	2	5	8

2.1.6 Final mesh analysis

The main mesh quality test results are here presented:

a. Cell base size: 21 mm. The more accurate base size analyzed, as expected, presented the lowest local relative errors in a general comparison of all parameters.
b. Surface growth rate: Fast. Given that the more accurate base size was chosen, it is possible to choose a less favorable surface growth rate, as the local errors in the tests reach approximately 1%.
c. Volumetric growth rate: Fast. Similar to the surface growth rate, the local relative errors of this parameter are in the order of 1% and are considered small. Therefore, choosing a faster growth rate that would lead to shorter processing time is valid.
d. Wake refinement: 100%. The wake refinement parameter produced the lowest local and global errors, making it the parameter with the least influence on the final result.
e. Number of prism layers: 5. This parameter showed significant influence on the simulation results, second only to the base size. In an attempt to obtain better results without excessive computational power requirements, a moderate configuration was chosen in this case.

Using the provided mesh settings, a y^+ value verification was conducted. y^+ is a non-dimensional parameter used to evaluate the adequacy of wall spacing for the selected wall treatment. The y^+ analysis within the final mesh settings

demonstrates that the majority of cells have y^+ values ranging from 1 to 30, indicating appropriate mesh refinement (Siemens, 2021).

According to the parameter settings outlined in the summary above, the computer employed for executing the simulations in this study adheres to the following primary specifications: an NVIDIA GeForce GTX 1650 4 GB graphics card and a 9th generation Intel Core i5 processor. Using this computer, the average simulation duration, in accordance with the study's objectives, approximates 2.5 hours.

Additionally, a separate set of simulations was conducted with a computer with an NVIDIA GeForce RTX 3060 12 GB graphics card and an 11th generation Intel Core i7 processor, aimed at comparative analyses of mesh quality. This enabled the execution of more computationally intensive simulations for comparison with the previous results. Meshes were generated with a base size of 7 mm, slow surface growth rate, and slow volumetric growth rate. The minimum cell size was adjusted to 30% instead of the previous 10% due to observed solution divergence for smaller cells. Thus, meshes of approximately 3 million cells were obtained, which were tested only for velocities of 0.25 m/s and 1.25 m/s, and for angles of 0° and 90°, totaling 4 simulations aimed at evaluating the extremes of the analysis range.

2.2 Post-Processing

To calculate the drag force, it is necessary to first generate a force report. In order for the report to display the desired data, it is necessary to configure the force direction vector, the force unit in Newtons, and the region of interest for the calculations, which is the surface of the ROV body.

It is important to note that in order to calculate drag, for example, using the force calculation in STAR-CCM+, it is necessary to specify the force direction vector in the direction of motion (Siemens, 2021). Since this study aims to calculate the drag force on the ROV body, the force direction vector is specified as [-1, 0, 0], as the flow is in the negative x-direction.

The force on a surface is calculated by the software using the following equation:

$$F_s = \sum_f \left(f_f^{pressure} + f_f^{shear}\right).n_f \tag{1}$$

where $f_f^{pressure}$ and f_f^{shear} are the pressure and shear stress vectors that the fluid exerts on the surface, and n_f is a user-specified direction vector that indicates the direction in which the force will be computed. This study represented an initial investigation that focused on determining drag parameters; the calculation of lift force was not within the scope at this stage.

2.3 Design Manager

The Design Manager is a STAR-CCM+ internal module that provides an automated approach to perform design exploration studies, including performance evaluation and optimization (Siemens, 2021). The Design Manager allows users to evaluate multiple cases of a predefined analysis (denominated as reference) by modifying various variables, whether they are associated with 3D model parameters or involved physical models, scalars, or vectors. The diagram presented at Figure 8 provides an overview of the analysis workflow employing the Design Manager in Simcenter STAR-CCM+.

The use of Design Manager facilitates the variation of pre-established parameters as variables throughout this work, such as the platform locomotion speed and the rotation angle around the platform's z-axis. Therefore, it is possible to define a total of 8 studies, with 7 of them related to the variation of ϕ from 0° to 90°, equally spaced, and the last one related to the study of motion along the z-axis.

The study is then conducted by varying the speed from 0.25 m/s to 1.25 m/s, equally spaced, for each of the 8 studies created in the Design Manager, resulting in a total of 40 analysis cases. The main response sought for each study is the drag force obtained in each analysis. Additionally, the drag coefficient and the total simulation time were also requested as responses.

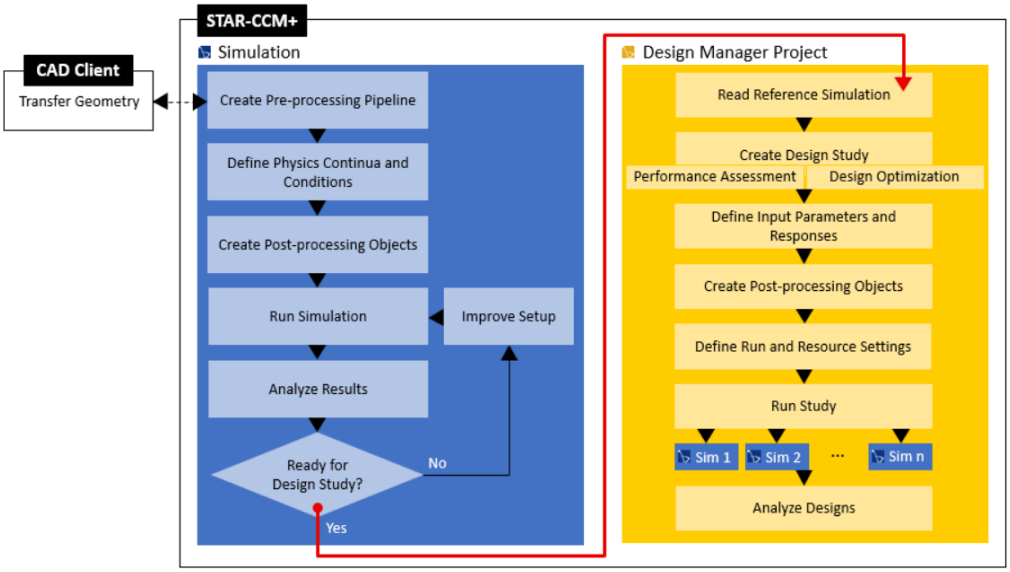

Figure 8. Analysis process in Design Manager. Source: Siemens (2021, STAR-CCM Software Help 2021).

3. RESULTS AND DISCUSSION

For each analyzed rotation angle of the platform, 5 different force results were obtained, corresponding to platform (or fluid) speeds of 0.25, 0.5, 0.75, 1.0, and 1.25 m/s. Therefore, for each of the 8 studies, it is possible to generate a curve connecting the 5 points formed by the composition $(x, y) = (V, F_d)$, where V is the analysis speed and F_d is the drag force. Thus, the corresponding drag force for any speed between 0.25 and 1.25 m/s can be determined through the generated polynomial interpolation curve. The speeds were defined within a lower limit close to 0 m/s and an upper limit slightly above the maximum speed found by Marques and Catarin (2020), approximately 0.9 m/s.

In this regard, an internal module of the MATLAB software (from MathWorks) known as Curve Fitting Toolbox or CFTOOL was used. The module provides an application and functions for fitting curves and surfaces to given input data (Mathworks, 2020). The generated polynomial interpolation curves for all angles can be visualized in Figure 11.a, and their parameters are shown in Table 3.

Table 3. Parameters of the polynomial interpolation curves for each angle ϕ. Source: Marques (2022, p. 69).

Parameter	ϕ = **0°**	ϕ = **15°**	ϕ = **30°**	ϕ = **45°**	ϕ = **60°**	ϕ = **75°**	ϕ = **90°**
$p1$	14,09	9,04	3,63	-9,26	1,71	-5,23	3,69
$p2$	-34,47	-26,52	-10,90	24,27	-6,84	13,14	-15,63
$p3$	60,78	62,44	49,46	25,08	63,07	47,63	77,15
$p4$	-7,78	-8,50	-1,82	11,29	-0,38	7,31	-4,27
$p5$	0,92	1,20	0,36	-1,32	0,19	-0,78	0,70

It is then possible to calculates the drag force for any velocity between 0.25 and 1.25 m/s for a study of ϕ between 0 and 90° with a fixed increment of 15°, as the equation below:

$$f(V) = p1.V^4 + p2.V^3 + p3.V^2 + p4.V + p5, \quad (2)$$

where the parameters are defined according to Table 3.

As observed in Figure 9.a, the polynomial curves demonstrate that the drag force increases with the increase of the analyzed angle, which was expected since the increase of ϕ implies an increase in the projected frontal area in relation to the flow direction. It is also evident that there is no standardized variation of the drag force between consecutive 15° increments.

The further set of simulations performed with a computer of superior hardware specifications allowed the execution of more computationally intensive simulations, enabling a comparative analysis of meshes of approximately 930 thousand cells with meshes of 3 million cells, using the same physics model. The results obtained by the solver ranged from 0.04%

to 4.56% in terms of relative errors compared to the 930 thousand cells meshes, validating the previously obtained results and demonstrating that the mesh quality study provided reasonable approximations.

The obtained results from the simulations can also be compared with the analytical result obtained by Marques and Catarin (2020). The calculation of the force obtained for two fully open nozzles resulted in a maximum of 56.58 N. By obtaining the x-component of this vector, a maximum force of 25.25 N is identified, resulting in a velocity of 0.9 m/s according to the authors. However, based on Figure 9.a, for an angle of 0°, it can be observed that the equivalent velocity for the same drag force obtained in this study is approximately 0.87 m/s. This suggests that the velocity results obtained by the authors were slightly overestimated or, in other words, the drag force was underestimated.

Some considerations should still be taken into account, such as the fact that the drag force estimate calculated by the authors did not yet consider the area generated by the nozzles, which, at an angle of 63.5°, generate a considerably larger frontal area compared to the same nozzles at 0°, and therefore had been disregarded. Thus, the drag force found by the authors may have been lower than the actual force experienced in reality and by the simulation.

Finally, a surface was generated with the aim of obtaining a function $f(V, \phi)$ that, given a relative motion velocity between the ROV and the fluid in the range of 0.25 to 1.25 m/s V and any angle between 0° and 90° ϕ, returns the drag force Fd. Using the CFTOOL once again, the surface $f(V, \phi, Fd)$ can be obtained as shown in Figure 9.b through a 4th-degree polynomial interpolation in V and a 3rd-degree polynomial interpolation in ϕ. The final equation for this surface is presented below, in Equation (3).

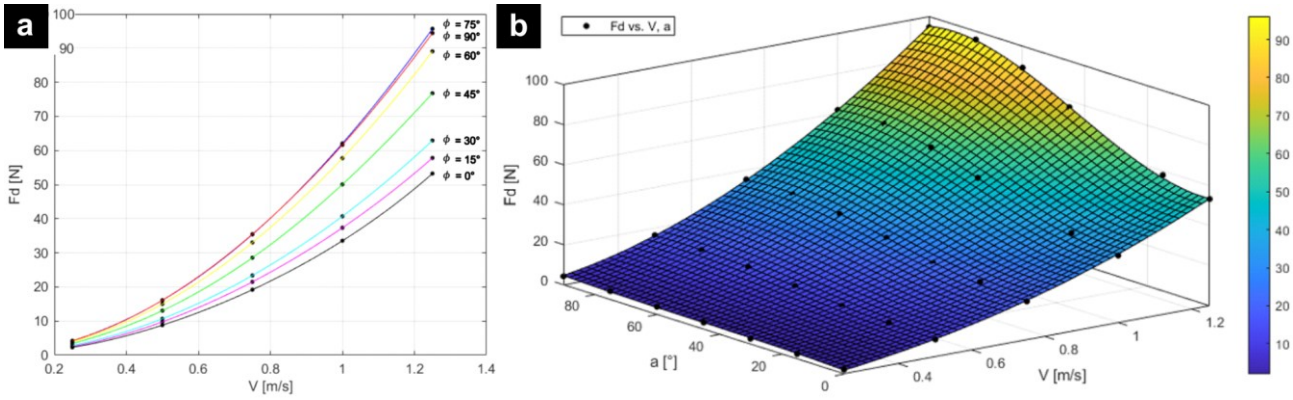

Figure 9. Polynomial interpolation curves for the analyzed angles (a) and surface $f(V, \phi, Fd)$ obtained from the analyses (b). Source: Adapted from Marques (2022, p. 68 and 72).

$$f(V,\varphi) = -1.4 + 6.1\,V + 0.25\,\varphi + 30.54\,V^2 - 0.84\,V\varphi - 0.01\,\varphi^2 - 3.42\,V^3 + 0.58\,V^2\varphi + 2x10^{-3}\,V\varphi^2 + 5.55x10^{-5}\,\varphi^3 + 2.52\,V^4 - 0.11\,V^3\varphi - 4.78x\,10^{-4}\,V^2\varphi^2 - 1.8x10^{-4}V\varphi^3 \quad (3)$$

4. CONCLUSIONS

The difficulty in reproducing experimental tests and trials in test tanks for complex geometry ROVs or AUVs promotes the development and use of alternative methods for estimating drag forces on these vehicles. This is not only due to the geometric challenges involved but also for cost reduction purposes.

The use of CFD techniques demonstrated throughout the work has proven to be viable in various stages of a design process, specifically as a valuable source of information for the progression of the project. In other words, the ease with which results can be obtained through CFD can be leveraged to benefit a project by enabling early changes prior to a final version, without the inclusion of significant expenses associated with physical experiments.

In this work, the hydrodynamic parameters were identified for the subsea platform in a steady-state regime. A study was conducted on the mesh quality used in the simulation, which led to the configuration of the parameters used for mesh generation in the simulations. The forces and drag coefficients for the platform translations were obtained through CFD simulations, enabling the creation of a surface that relates the platform's drag force to the analyzed velocities and angles. Finally, this surface was compared to the previous results obtained by Marques and Catarin (2020).

One of the next steps is to analyze the influence of the umbilical cable on the platform, which is essential for supplying power to the internal components of the ROV system. Since this work focuses on the initial analysis of the hydrodynamic modeling of the platform using CFD software, the analysis of the ROV and umbilical cable assembly was not considered. However, the cable can introduce not only drag but also have an influence on the overall hydrodynamics of the platform, potentially affecting how the controls respond to these stimuli. This opens up an opportunity for future work involving a more detailed analysis of the ROV and umbilical system.

Finally, this work presents the hydrodynamic model of the platform in a steady-state regime. It would be interesting, in the future, to obtain the hydrodynamic model in a transient regime, which would involve a more complex analysis of the equations involved.

5. ACKNOWLEDGMENT

We extend our gratitude to the Naval Simulation Laboratory (LaSiN) and the Underwater Technology Laboratory (LaSub), as well as all their members, for the resources and contributions to the development of this work.

6. REFERÊNCIAS

Achenbach, E. Experiments on the flow past spheres at very high Reynolds number. Journal of Fluid Mechanics, vol. 54, p. 565-575, 1972.

Cely, J.S., Saltaren, R., Portilla, G., et al. Experimental and Computational Methodology for the Determination of Hydrodynamic Coefficients Based on Free Decay Test: Application to Conception and Control of Underwater Robots. 2019. Sensors, 19(17), 3631. doi.org/10.3390/s19173631.

Chin, C and Lau, M. Modeling and testing of hydrodynamic damping model for a complex-shaped remotely-operated vehicle for control. J. Marine. Sci. Appl. 11, p. 150–163, 2012. https://doi.org/10.1007/s11804-012-1117-2.

Constantinescu, G.S and Squires, K.D. LES and DES investigations of turbulent flow over a sphere. AIAA Paper 2000-0540, 2000.

Constantinescu, G.S., Pacheco, R., Squires, K.D. Detached-Eddy simulation of flow over a sphere. AIAA, Aerospace Sciences Meeting, Paper 2002-0425, 2002.

Fox, R.W., Pritchard, P.J., Mcdonald, A.T. Introduction to fluid mechanics (*in Portuguese*). 7. ed. Rio de Janeiro: Ltc, 2011.

Gong, J., Wu, Z., Ding, J., et al. Numerical analysis of propulsion performance of a waterjet-propelled vehicle in steady drift. Ocean Engineering, [S.L.], v. 266, p. 113136, dez. 2022. Elsevier BV. http://dx.doi.org/10.1016/j.oceaneng.2022.113136.

Grewal, M.S., Weill, L.R.; Andrews, A.P. Global Position System, Inertial Navigation and Integration. New York, USA. John Wiley & Sons. 2001.

Hu, H.H. Computational fluid dynamics. In: Kundu, P.K. and Cohen, I.M. Fluid Mechanics. 4. ed. Burlington: Elsevier, p. 411-464, 2008.

Kim, D. and Choi, H. Laminar flow past a sphere rotating in the stream wise direction. Journal of Fluid Mechanics, vol. 461, p. 365-386, 2002.

Marques, A.S. and Catarin, H.V. Design and control of an underwater platform with jet propulsion (*in Portuguese*). Joinville, 2020. Report (Scientific Initiation) - Naval Engineering Course, Federal University of Santa Catarina, Joinville, 2020.

Marques, A.S. CFD model for determining the drag of a steady state ROV (*in Portuguese*). 2022. 87 f. TCC (Graduation) - Naval Engineering Course, Federal University of Santa Catarina, Joinville, 2022. Available in: https://repositorio.ufsc.br/handle/123456789/237362. Accessed on: 01 Jun. 2023.

Muniz, L.A.R. Finite volume method applied to two-dimensional flow problems in the inlet region of cylindrical pipelines (*in Portuguese*). 1995. Dissertation (Master in Chemical Engineering) - Chemical Engineering Course, Unicamp, Campinas, 1995.

Ramírez-Macías, J.A., Brongers, P., Rúa, S., et al. Hydrodynamic modelling for the remotely operated vehicle Visor3 using CFD. 2016. IFAC-PapersOnLine, 49(23), 187–192. doi.org/10.1016/j.ifacol.2016.10.341.

Siemens Digital Industries Software. Simcenter STAR-CCM+ User Guide, version 2021.2.

Tavares, A.M, Gomes, S.C.P, Cunha, M.A.B. Dynamic modeling and control of an underwater vehicle (*in Portuguese*). Vetor, Rio Grande, v. 15, n. 2, p. 101-116, 2005. Available in: http://repositorio.furg.br/handle/1/3377. Accessed on: 05 May. 2022.

The Mathworks Inc. MATLAB. 2020. version 9.8.0 (R2020a). Natick, Massachusetts.

Yuh, J. Design and control of autonomous underwater robots: A survey. Autonomous Robots, v. 8, n. 1, p. 7-24, 2000.

Zanoni, F.D. Modeling and implementation of the navigation system for an AUV (*in Portuguese*). 2012. Dissertation (Master in Engineering) - Mechanical Control and Automation Engineering Course, Polytechnic School, University of São Paulo, São Paulo, 2012. Available in: https://www.teses.usp.br/teses/disponiveis/3/3152/tde-23032012-114741/publico/Dissertacao_Fabio_Doro_Zanoni.pdf. Accessed on: 05 May 2022.

7. RESPONSIBILITY NOTICE

The authors are the only responsible for the printed material included in this paper.